Journal of Computational Neuroscience 19, 39–51, 2005

Fractal Stochastic Modeling of Spiking Activity in Suprachiasmatic Nucleus Neurons

SUNG-IL KIM, JAESEUNG JEONG AND YONGHO KWAK
National Creative Research Initiative Center for Neurodynamics and Department of Physics, Korea University, Seoul 136-701, South Korea

YANG IN KIM AND SEUNG HUN JUNG
Department of Physiology and Neuroscience Research Institute, Korea University College of Medicine, Seoul 136-701, South Korea

KYOUNG J. LEE
National Creative Research Initiative Center for Neurodynamics and Department of Physics, Korea University, Seoul 136-701, South Korea
kyoung@nld.korea.ac.kr

Received February 2, 2004; Revised November 30, 2004; Accepted December 9, 2004

Action Editor: Carson C. Chow

Abstract. Individual neurons in the suprachiasmatic nucleus (SCN), the master biological clock in mammals, autonomously produce highly complex patterns of spikes. We have shown that most (∼90%) SCN neurons exhibit truly stochastic interspike interval (ISI) patterns. The aim of this study was to understand the stochastic nature of the firing patterns in SCN neurons by analyzing the ISI sequences of 150 SCN neurons in hypothalamic slices. Fractal analysis, using the periodogram, Fano factor, and Allan factor, revealed the presence of a 1/f-type power-law (fractal) behavior in the ISI sequences. This fractal nature was persistent after the application of the $GABA_A$ receptor antagonist bicuculline, suggesting that the fractal stochastic activity is an intrinsic property of individual SCN neurons. Based on these physiological findings, we developed a computational model for the stochastic SCN neurons to find that their stochastic spiking activity was best described by a gamma point process whose mean firing rate was modulated by a fractal binomial noise. Taken together, we suggest that SCN neurons generate temporal spiking patterns using the fractal stochastic point process.

Keywords: suprachiasmatic nucleus, interspike intervals, fractal, stochastic, gamma point processes, long-term correlations

1. Introduction

The SCN is a hypothalamic region that contains the circadian pacemaker in mammals (Meijer and Rietveld, 1989; Morin, 1994). The core mechanism underlying the generation of the circadian rhythms is thought to be the transcription- translation feedback loops of clock genes, such as *Per*, *Clock*, *Bmal*, and *Cry* (for reviews, Reppert and Weaver, 2001, 2002). It is surmised that a substance (or substances) from the core loop transmits its circadian signal to cellular functions like neuronal discharge or release of diffusible factors, and

consequently spiking patterns of individual SCN neurons exhibit higher mean firing rates during the day and lower firing rates at night (Inouye and Kawamura, 1979; Jagota et al., 2000; Schaap et al., 2003). In other words, the circadian rhythm of SCN neurons is expressed by the sinusoidal modulation of their mean firing rates. Such circadian oscillation in firing frequency is known to be crucial for the transmission of time information to other brain areas to impose circadian rhythmicity on physiological and behavioral activities (Schwartz et al., 1987; Newman et al., 1992; Shirakawa et al., 2001).

On a short time scale, however, the spiking activity of individual SCN neurons is neither periodic nor modulated. The spontaneous firing rate of an SCN neuron incessantly varies ranging from 1.5 to 15 Hz, often accompanied by intermittent bursts (Gillette, 1991; Pennartz et al., 1998; Jagota et al., 2000; Schaap et al., 2003). In fact, interspike intervals (ISIs) of SCN neurons are quite irregular and complex. So far, how this complex sequence of action potentials operating on a fast time scale relates to the circadian signal of mean firing rates varying over a much slower time scale and to the molecular clockwork of the SCN is unknown.

As an effort to provide answer to this important, challenging question, we have performed nonlinear time series analyses on an extensive set of the ISI data recorded from SCN cells in slice preparations and found that about 90% of the SCN cell population generated stochastic patterns of spikes, while the remainders exhibited nonlinear determinism (Jeong et al., submitted). This finding in turn motivated us to investigate the very nature of the stochastic process underlying the irregular spiking activity of SCN neurons.

Neural spike trains, in general, have often been viewed as a stochastic signal of some renewal processes showing absolutely no correlation among their ISIs (Cox and Lewis, 1966; Tuckwell, 1989). Such a description has been quite accurate in several different occasions (Levine, 1980; Steedman et al., 1983; Steedman and Zachary, 1990). The spiking activity of SCN neurons, however as we will show in detail, does not follow a simple renewal process but a more complex, yet, well-defined stochastic process known as a fractal point process.

The hallmark of the fractal point process is the presence of long-term correlations. The spike train generated by the fractal point process exhibits a self-similar or scale-free behavior—in other words, no characteristic time scales dominate the dynamics of the underlying spiking process. The simplest scale-free relationship is a power-law: a straight line appears on a log-log plot of a dependant variable (e.g. the number of ISIs) versus an independent variable (e.g. the magnitude of ISIs). The scale-free behavior indicates that long lasting correlations are present in the signal, extending over the entire range of time scales (thus, long-term correlation). In the present study, using statistical and fractal measures, we showed that SCN neurons truly followed the fractal stochastic process.

We also investigated the role of GABA, the primary neurotransmitter of the SCN, in the observed fractal behavior. The $GABA_A$ receptor antagonist bicuculline was applied to SCN neurons to block $GABA_A$ receptor-mediated synaptic couplings and to see if any changes arose in the fractal behavior of the ISI sequences. The fractal behavior was found persistent in the ISI sequences after the bicuculline application, indicating that the observed fractal behavior pertains to individual SCN neurons or originates from non-synaptic cell-to-cell coupling interactions.

2. Materials and Methods

2.1. Animals and Brain Slice Preparation

Male Sprague-Dawley rats ($n = 46$; 40–100 g) were housed in a temperature-controlled room (22–24°C) under a 12/12-hr light/dark cycle (light on 07:00–19:00) for at least 2 weeks prior to use. The rats were anesthetized with Nembutal (6 mg/100 g body weight) in the daytime of subjects, and then the brains were quickly removed and submerged in ice-cold artificial cerebrospinal fluid [ACSF (mM): 124 NaCl, 26 $NaHCO_3$, 3 KCl, 2.4 $CaCl_2$, 1.3 $MgSO_4$, 1.25 NaH_2PO_4, 10 Glucose, 95% O_2, and 5% CO_2 saturation]. Using a vibrating tissue slicer (Vibratome 1000, Technical Products International, USA), a block of hypothalamic tissue was cut into slices coronally at the thickness of 120–150 μm. The slices containing the SCN were transferred to a recording chamber perfused by the same ACSF at the flow rate of 1.0–1.5 ml/min. The experimental procedures described above were in accordance with the guideline set by the Korea University College of Medicine Animal Research Policies Committee.

2.2. *Extracellular Recording*

After 1-hr incubation in the recording chamber, extracellular recordings were performed at room temperature (25–27°C). The recording electrodes made of borosilicate tubings (Sutter Inst. Co. USA) had a tip diameter of 2–4 μm with a resistance of 3–5 Mohm. Cell-attached patch (CAP) configuration without membrane rupture was achieved for extracellular single-unit recording. In a CAP mode, a single action potential caused a transient capacitive current over the patch of membrane sucked into the pipette tip. This was recorded under voltage clamp conditions with a pipette potential of 0 mV. The recordings were performed using Axo-patch 200B amplifier (Axon Instruments, USA) in track mode from 150 SCN neurons for 20–40 minutes, and the ISI data were stored using pClamp software. The mean number of data points was $6,288 \pm 3,001$ (range: 1,422–19,778). For each recording, first two minute of data were discarded to ensure the stationarity of the ISI sequences as possible.

2.3. *Fractal Stochastic Analysis*

The ISI histogram was used to measure the relative frequency of occurrence $p_\tau(\tau)$ of an ISI τ. It is an estimate of the probability density function of ISI magnitudes. Although its construction yields the loss of information about temporal ordering of spikes, and thus dependencies among intervals, the ISI histogram with its skewness (SK) and coefficient of variance (CV) provides some clues for identifying the underlying stochastic process of the data.

To examine the presence of long-term correlations in ISI patterns of SCN neurons, the periodogram, Fano factor, and Allan factor were estimated. These statistical measures provide a way of investigating if a given data set has a self-similarity property. If their values estimated over brief periods of time are proportional to those estimated over longer periods, SCN neurons prove to exhibit a power-law (scale-free) behavior within ISI patterns, which is the hallmark of a fractal behavior.

The periodogram (PG) estimates power spectral density (PSD) of the ISI sequences. For fractal signals, the PG exhibits a power-law behavior that varies with the frequency as $S(f) \propto f^{\alpha_P}$, particularly in the low frequency range. The Fano factor (FF) is the ratio of the variance of the number of spiking events in a counting number to the mean. The FF of a fractal stochastic process takes the power-law form $T^{\alpha_F} (0 < \alpha_F < 1)$ for large counting time T, while it tends to stay in a constant value independent of T for a renewal process. The α_F is considered as the fractal exponent (scaling exponent) of the point process. The power-law form T^{α_F} implies that the fluctuations in the firing rate converge relatively slowly as T is increased, endowing an evidence for self-similarity and long-term correlations within the ISI sequence. Although the FF can detect the presence of the fractal behavior, mathematical constraints prevent it from increasing with the counting time faster than T^1. Therefore, it seems to be unsuitable as a measure for fractal exponents greater than unity (Lowen et al., 2001). For the reliable estimation of a fractal exponent that may assume a value greater than unity, we additionally used the Allan factor (AF), which is a measure whose increase is not constrained as it is for the FF. The detailed concepts and estimation algorithms of these measures are presented in the Appendix.

The surrogate data test was used to confirm the presence of power-law characteristics in the ISI sequences of SCN neurons. Surrogate data are a randomized sequence of the original data with any long-term correlations or power-law relationship destroyed (Schreiber and Schmitz, 2000). Statistically significant differences in the fractal exponents of the original data and their surrogate data would imply the presence of long-term correlations (power-law relationship) in the original data. In our analysis, the fractal exponent estimation (α_P, α_F, and α_A) was applied to each raw ISI data set and its 19 different versions of surrogates. To quantify the significance of the fractal behavior, the significance S was introduced (Longtin, 1993; Shen et al., 2003). The S was defined by

$$S = \frac{|<\alpha_s> - \alpha|}{\sigma_s}, \tag{1}$$

where $<\alpha_S>$ denotes the mean value of the fractal exponent of the 19 surrogate data, α is the fractal exponent of the original data set, and σ_s is the standard deviation of the fractal exponents of the surrogates. If any fractal structure exists, α should be significantly greater than $<\alpha_S>$. An S-value larger than 1.96 indicates the presence of fractal behavior in the original data (with a 0.95 level of significance), as suggested by Shen et al. (2003). All numerics were expressed by mean $\pm$ S.D. All tests of statistical significance were two-tailed.

2.4. Statistical Analysis

A goodness-of-fit test for various computational models was performed using the Kolmogorov-Smirnov Test, which compares the ISI histograms of the ISI sequences obtained from the SCN neurons and ISI distributions generated the homogeneous Poisson process, the dead-time-modified Poisson point process, the gamma renewal process, and fractal stochastic process. The Kolmogorov–Smirnov test measures the maximum difference between the cumulative distribution functions of the models and of observed data and calculates the probability that the two distributions would exhibit a difference at least that large if the samples were drawn from identical populations. We find the greatest discrepancy between the observed and expected cumulative frequencies, which is called the D-Statistic, and compare this against the critical D-Statistic for that sample size. If the calculated D-Statistic is greater than the critical one, then reject the null hypothesis that the distribution is of the expected form.

3. Results

3.1. ISI Histograms of SCN Neurons

ISI sequences from 150 SCN neurons recorded in 46 SCN slices were analyzed. Most neurons had ISIs with a unimodal distribution with a mean interval of 0.27 ± 0.11 sec (range: 0.05 to 0.9 sec). The long tail was present in the long ISI range of the histogram. Figure 1 presents the ISI histogram for the neural spike train recorded from a typical SCN neuron. For the surrogate data, the ISI histograms and consequently the CV and SK were the same as those of the original data, because random shuffling of the ISIs did not alter the distribution of the intervals (Table 1).

The most suitable stochastic model for describing the ISI histograms of the SCN neurons was investigated. The homogeneous Poisson process (HPP), fixed-dead-time-modified Poisson point process (DTMP), and gamma renewal process (GRP) were tested as a candidate (see Appendix for their definitions). In Fig. 1, the ISI histogram of the experimental data was compared with two of the simulated data, one generated by the DTMP and the other by the GRP with proper μ and r. (The HPP case is not shown, because it is just a parallel-shift of the DTMP.) Neither the HPP nor the DTMP proved suitable for matching the shape of the ISI histogram associated with the SCN neurons (Kolmogorov–Smirnov test, $D = 0.056, P < 0.0001$). By contrast, the GRP offered a good fit, except for the asymmetric long tail in the long ISI region (see the inset of Fig. 1). Two parameters, μ and r, of the GRP probability density function were obtained from the relationships between the CV and mean ISI and the parameters ($\mu = 1/<\tau>, r = 1/CV^2$). The parameters determined by the CV and mean ISI of the data had wide ranges: $2 \leq r \leq 56$ and $1.24 \leq \mu \leq 10.98$.

Table 1. The mean and standard deviation (SD) values of statistical and fractal measures for the 150 SCN neurons and their surrogate data. The S-scores of the fractal measures greater than 3 indicates the presence of the fractal behavior within ISIs of the SCN neurons.

	SCN neurons ($n = 150$)	Surrogate data ($n = 2850$)	S-scores
SFR	4.67 ± 1.57	4.67 ± 1.57	0
CV	0.38 ± 0.20	0.38 ± 0.21	0
SK	1.48 ± 1.97	1.48 ± 1.96	0
α_P	0.85 ± 0.35	0.03 ± 0.20	5.96 ± 3.34
α_F	0.68 ± 0.20	0.03 ± 0.15	6.50 ± 2.63
α_A	0.81 ± 0.38	0.06 ± 0.19	6.56 ± 2.74

SFR: spontaneous firing rate.

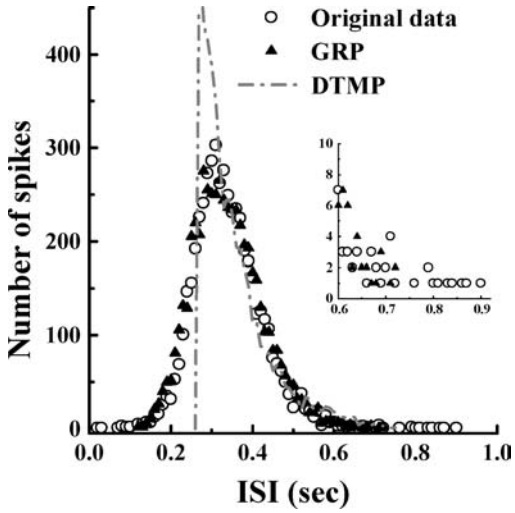

Figure 1. ISI histograms for the original data recorded from a typical SCN neuron (o) and for the simulated data generated from the GRP (▲) and DTMP (—·—·—). The GRP provides a good fit in most parts except for the long-tail region, while the DTMP severely fails to describe the ISI distribution of the SCN neuron, in particular on the short ISI region. The inset illustrates the failure of GRP to simulate the longer part of ISIs beyond the marker (↓).

Although the ratio of the SK to CV is exactly 2 for the GRP (Shinomoto et al., 1999), the mean ratio for the 150 SCN neurons was found to be 3.42 ± 4.04 ($SK = 1.63 \pm 1.97$, $CV = 0.37 \pm 0.18$). This result indicates that the ISI histogram of the data is more skewed than that of the GRP. This discrepancy seemed to arise from the asymmetric long-tailed part of the distribution in the long ISI region. To test the fitness of the GRP as a model for the ISI distribution of the SCN neurons quantitatively, we quantified the difference in the ISI distributions generated from GRP and from SCN neurons using the D-statistic from the Kolmogorov–Smirnov test. The ISI distribution of GRP process exhibited a significant difference in the ISI histogram of observed data ($D = 0.022$, $P < 0.05$), although the GRP provides a good fit to the ISI histogram for the SCN neurons except for long ISIs.

3.2. *Fractal Behavior of SCN Neurons*

For the estimation of the periodogram (PG), the data set was divided into $T = 500$ sec. Each of these segments was subdivided into $M = 8{,}192$ (2^{13}) bins, and within each bin the number of spikes was counted. Compared with the observed ISIs, the bin size (0.061 sec) was so short that most bins contain at most one spike. The fast Fourier transform was performed on those binary sequences. We obtained the PG over the ranges $1/T = 0.002$ to $M/2T = 8.19$ Hz.

The PG of the original data recorded from a typical SCN neuron and that of their surrogate data are presented in Fig. 2(A) on a log-log scale. The PG of the original data exhibited a $1/f$-type power-law behavior, in particular in low-frequency region (i.e. long-time range), whereas the PG of the surrogate data showed the flat white-noise like behavior in the same range. Regression analysis was used to calculate the slope of a power-law relationship. The average slope—i.e. the fractal exponent α_P—of the ISI data for the 150 neurons was found to be 0.85 ± 0.35, while that of the surrogate data was 0.03 ± 0.20. The S scores for the α_P larger than 3 clearly support the presence of the power-law behavior within ISIs of the SCN neurons (Table 1).

As another measure, the FF of the ISI data was estimated for the neurons and their surrogate data. The counting time T was increased from 0.1sec with a step of 0.1 sec. Figure 2(B) shows the FFs of the ISI data for an SCN neuron and the corresponding surrogate data on a log-log plot. For the small T region, the FF of the ISI data dipped below one and went through

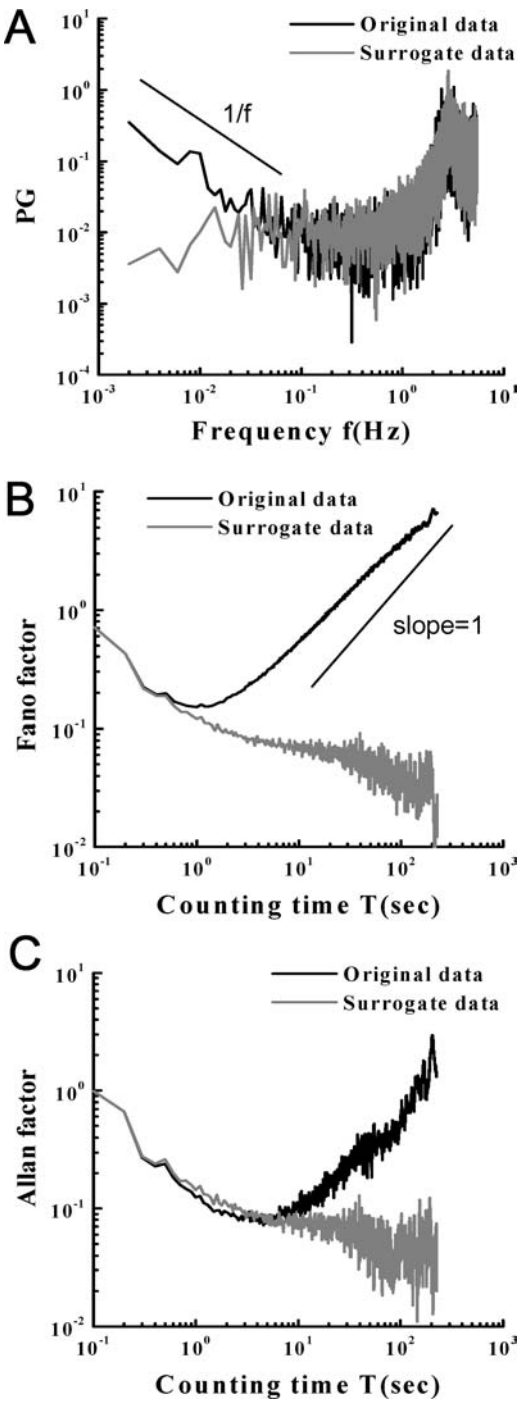

Figure 2. Estimation of long-term correlations of the original data recorded from a typical SCN neuron and their surrogate data on a log-log plot. A: the PG shows a $1/f$-type power-law behavior in the low-frequency region. B: The FF increases in a power-law fashion in the large counting time T. C: The AF also increases in a power-law fashion in the large counting time. For each measure, the power-law behavior is removed in the randomly shuffled surrogate data.

the nadir point around the mean ISI. It can be understood as that the deviation of the number of spikes in successive bins is least at the mean ISI. Then the FF value of the original data diverged in the power-law form, indicating the presence of long-term correlations among ISIs, whereas the surrogate data did not show the power-law behavior. The mean fractal exponent obtained from the FF curves of the 150 SCN neurons was $\alpha_F = 0.68 \pm 0.20$, which was significantly different from that of surrogate data ($\alpha_F = 0.03 \pm 0.15$). In the case of renewal processes, the FF asymptotically converges to a constant value of CV^2. The surrogate data exhibited the flat FF curve in the range of 10^0–10^2, as illustrated in Fig. 2(B).

Since the scaling power of the FF approached unity for some neurons, we estimated the Allan factor (AF) to ensure the presence of a fractal structure within the ISI sequences. The AF also exhibited a 1/f-type power-law behavior in long T region (Fig. 2(C)). The mean scaling exponent (α_A) was 0.81 ± 0.38, significantly larger than that of the surrogate data ($\alpha_A = 0.06 \pm 0.19$). The shared power-law characteristic of the FF and AF indicates that the SCN neurons exhibit the fractal behavior in the ISI sequences.

There was a good positive correlation between fractal measures. The Spearman correlation coefficient analysis revealed that the α_P was positively correlated with the α_F ($\rho = 0.66$), and α_A ($\rho = 0.6$), while the α_F was correlated with α_A ($\rho = 0.8$). These good correlations between the different measures clearly demonstrate the reliability of our findings.

Finally, the autocorrelation (AC) of the ISI data was estimated. Figure 3 presents the ACs of the ISI data for an SCN neuron and the surrogate data as a function of the time interval. While the surrogate data had stable values of the AC around zero, slowly decaying behavior was found in the AC profile of the ISI data. This result demonstrates the presence of slowly-decaying correlations in the ISI sequences of the SCN neurons. The correlation time length, typically defined as the first zero-crossing time of the AC, was approximately 50–150 sec.

3.3. The Bicuculline Effect on the Fractal Behavior

Since the GABA is the primary neurotransmitter of the SCN (Okamura et al., 1989; Moore and Speh, 1993), bicuculline was applied to investigate the role of $GABA_A$ receptor-mediated network couplings for the fractal behavior of the spiking activity of SCN

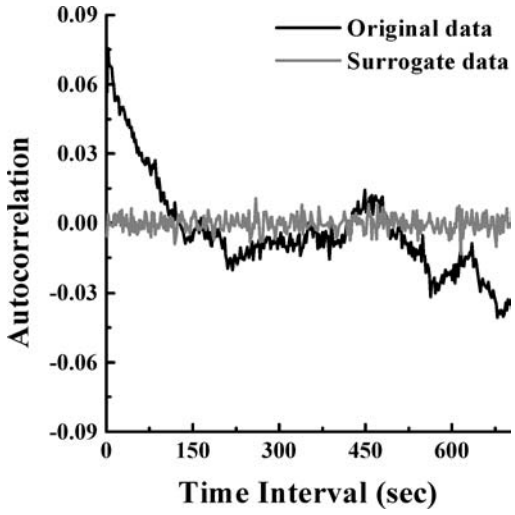

Figure 3. AC profiles for the original ISI data recorded from a typical SCN neuron and their surrogate data as a function of time. A slow decay and fluctuating behavior above zero in the AC profiles for a long time indicate the presence of long-term correlations within the data. The surrogate data, a series of uncorrelated random noise, exhibit flat AC profiles around zero independent of time.

neurons. Bath application of bicuculline (30 μM for 20 min) was performed in 56 neurons out of the 150 SCN neurons after the baseline recording (15–20 min) in a normal condition. Statistical and fractal measures of the 56 ISI data sets after the bicuculline application were compared with those of the data in normal conditions. The significant finding was that the power-law behavior was persistent after the bicuculline application as well illustrated in Fig. 4. This result indicates that the $GABA_A$ receptor-mediated synaptic coupling is not critical for the fractal behavior of SCN neurons. The detailed results are summarized in Table 2.

Table 2. Comparison of mean and SD values of statistical and fractal measures for the 56 SCN neurons and their surrogate data after the bicuculline application with those of normal conditions.

	Normal condition ($n = 56$)	Bicuculline condition ($n = 56$)	P
SFR	4.46 ± 1.36	5.76 ± 2.27	<0.05
CV	0.39 ± 0.25	0.48 ± 0.50	NS
SK	1.53 ± 2.58	2.41 ± 6.43	NS
α_P	0.97 ± 0.36	0.89 ± 0.37	<0.05
α_F	0.74 ± 0.17	0.60 ± 0.21	<0.05
α_A	0.86 ± 0.34	0.77 ± 0.40	<0.05

SFR: spontaneous firing rate, NS: not significant.

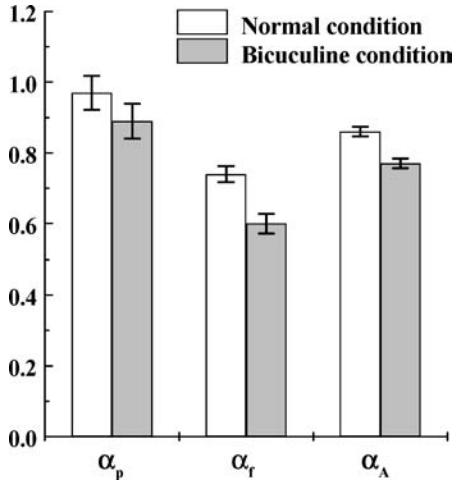

Figure 4. Comparison of mean fractal exponents and standard errors for the normal ISI data recorded from the 56 SCN neurons with those after the bicuculline application. (*:$P < 0.05$).

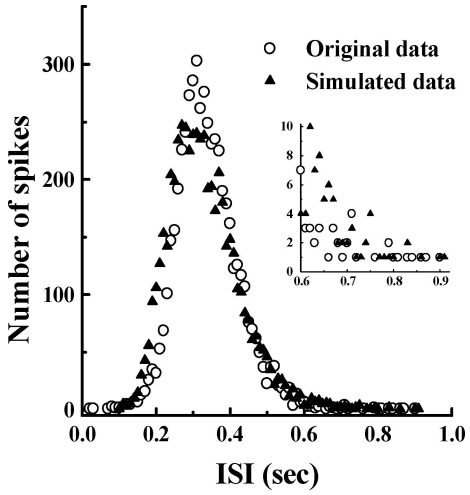

Figure 5. Comparison of ISI histograms for the original ISI data recorded from a typical SCN neuron (○) and their simulated data (▲). The agreement between two histograms is well particularly in the long tail part, as depicted in the inset.

3.4. A Computer Simulation for SCN Neurons

A computational simulation of the ISI sequences of SCN neurons was performed to faithfully reproduce the observed stochastic dynamics underlying the ISI patterns. The model should generate neural spike trains exhibiting the ISI histogram and long-term correlations among ISIs similar to those obtained from the experiments. Because the ISI histograms of the SCN neurons were well fitted by the GRP, an ISI sequence was generated from the GRP whose firing rate was modulated by fractal stochastic noise to impose long-term correlations among ISIs, so called a fractal-binomial-noise-driven doubly stochastic gamma (FBNDG) point process (see Appendix for the more-detailed model description). Figure 5 shows a good agreement between the probability density function of the simulated data and the ISI histogram of the real ISI data from a typical SCN neuron. The Kolmogorov–Smirnov test showed that the simulated data provide a good fit to the ISI histogram of SCN neurons ($D = 0.0095$, $P = 0.47$). Since the fundamental difference of the FBNDG from the simple GRP is the presence of long-term correlations among ISIs, the long-tail part of the ISI histogram is very likely associated with the long-term correlations.

The data presented in Fig. 2 were compared with those of simulated time series generated by the FBNDG in Fig. 6. The agreement was very good for all measures. The simulated data had very similar profiles and the fractal exponents of the periodogram, Fano factor, and Allan factor to those of the corresponding real data. It indicates that the FBNDG model is so far the best stochastic model for describing ISI patterns of SCN neurons.

4. Discussion

Stochastic properties of the firing activity recorded from SCN neurons in vitro have been examined using various statistical and fractal measures. ISI histograms of SCN neurons are very similar to those of gamma renewal processes with an order of 2–56 and with appropriate mean firing rates, except for the long tail part of the histogram. Fractal analyses using the periodogram, Fano factor, and Allan factor show the presence of a $1/f$-type power-law behavior in the neural spike trains of SCN neurons, which is the hallmark of a fractal process. The bicuculline experiments demonstrate that $GABA_A$ receptor-mediated synaptic interactions between SCN neurons do not play a critical role for generating the fractal behavior and thus the fractal stochastic activity is an intrinsic property of individual SCN neurons. The observed stochastic spiking activity of SCN neurons is best described by a gamma point process whose mean firing rate is modulated by a fractal binomial noise, the FBNDG model.

The origin of the fractal behavior in neural spike trains has been addressed by a number of researchers in different ways. Our observation that the fractal

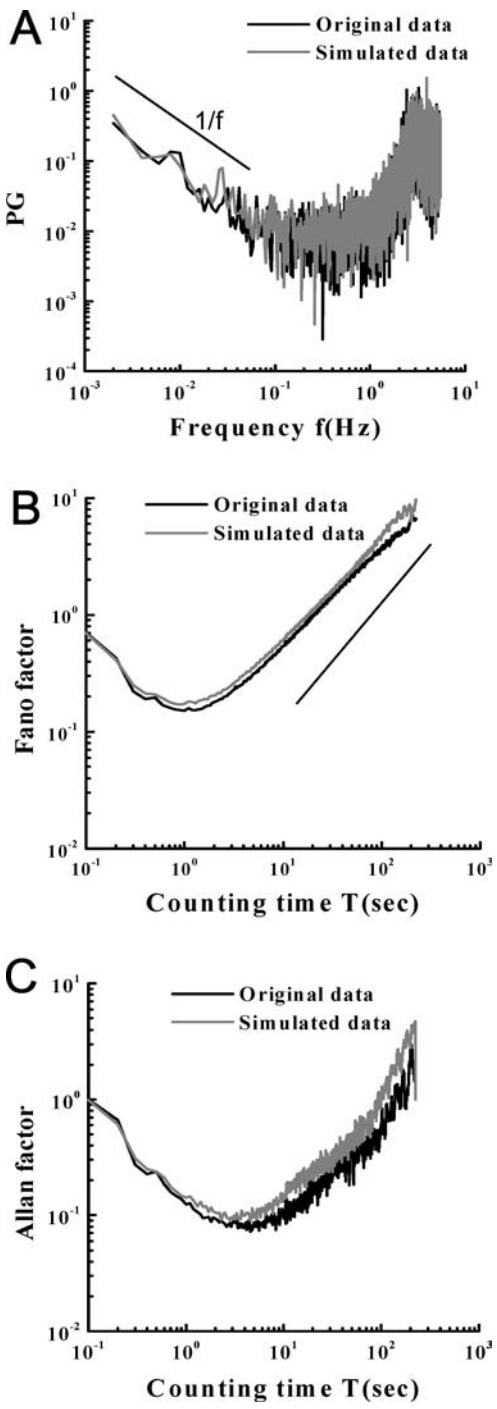

Figure 6. Comparison of fractal measures for the original data recorded from an SCN neuron with the corresponding simulated data generated from the FBNDG. The simulated data exhibit similar correlation properties to those of the original data, indicating that the FBNDG is very useful for describing the stochastic dynamics of the ISI firing pattern of the SCN neuron.

behavior is persistent during the synaptic blockade of SCN neurons by bicuculline suggests that the source of the observed fractal behavior pertains to the individual SCN neurons themselves. Soen and Braun (2000) also found a similar result in the spontaneous events of isolated heart cells. A possible source of the fractal behavior within each neuron is the fractal kinetics of ion channels, and consequently the fractal fluctuations in the membrane voltage (Lowen et al., 1999). Several studies have shown that ion channel opening and closing times in neurons exhibit the power-law behavior of a fractal process (Läuger, 1988; Liebovitch and Koniarek, 1992; Liebovitch and Toth, 1990, 1991; Millhauser et al., 1988). Using a Fitzhugh-Nagumo model, Lowen et al. (1999) have demonstrated that the fractal ion-channel gating activity can induce a fractal behavior in the firing rate. In some sense, the fractal binomial noise of the FBNDG process in our model mimics the fractal ion-channel behavior and the intracellular ionic concentrations as discussed by Lowen and Teich (1993). However, the time scale of the fractal ion-channel gating seems too rapid to produce the long-range correlations (hundreds of seconds) observed in the current study.

A more plausible source is the scaling of slow inactivation of ionic channels and their effect on spiking patterns at extended time scales. Many experiments and theoretical considerations suggest that an intrinsic activity-dependent gating mechanism of voltage-gated ion channels, and in particular slow recovery from inactivation of the channels might significantly contribute to long lasting modulations in neurons (Marom, 1998 and the references therein). Furthermore, Toib et al. (1998) have shown that the multiplicity of slow inactivation states in sodium channels is expressed as an intrinsic memory function that preserves traces of the previous activity over a wide range of time scales (a scale-free behavior) in the form of modulated reaction rates. However, the origin of fractal structure in ISI histograms of single neurons is still unknown and should be further investigated. In the case of SCN neurons, a slowly inactivating component of sodium currents is known to be involved in ionic mechanisms governing spontaneous firing (Pennartz et al., 1997). Thus, examination of the association between slow inactivation of ionic channels and the fractal behavior in firing patterns of SCN neurons will offer us insights as to intrinsic sources of the fractal behavior in SCN neurons.

However, the decrease in the fractal exponents with the bicuculline application does not exclude the

possibility that the $GABA_A$ receptor-mediated synaptic coupling, at least in part, contributes to the fractal behavior of SCN neurons. The involvement of the network coupling in generating the fractal behavior of neurons has been suggested in previous studies (West, 1990; Lowen et al., 1997). For the SCN, multiple ways of intercellular communications including gap junctional communication, neurotransmitter-based interactions, and ephaptic interactions have been reported (for reviews, van den Pol and Dudek, 1993; Colwell, 2000). These intercellular communications arise, of course, at various time scales ranging from msec (gap junction) to over 10 sec (calcium spikes). Therefore, neuronal interactions across multiple time scales as a whole can contribute to the fractal behavior in spiking patterns of SCN neurons. An immediate challenge for future is to investigate whether isolated SCN neurons exhibit a similar fractal behavior in their ISI patterns of spikes or to further explore the role of various neuronal interactions for the fractal behavior.

The functional role of the fractal structure in ISI histograms of SCN neurons is not clear. Long-term correlations and fractal behavior have been observed in patterns of action potential firings recorded in a variety of neuronal preparations including the auditory system (Kelly et al., 1996; Kumar and Johnson, 1993; Lowen and Teich, 1996; Powers and Salvi, 1992; Teich 1989), visual system (Teich et al., 1997; Turcott et al., 1995), somatosensory cortex (Wise, 1981), mesencephalic reticular formation (Grüneis et al., 1993), neocortex (Linkenkaer-Hansen et al., 2001, 2004), and medulla (Lewis et al., 2001). Although a few studies have reported the lack of the fractal behavior in neural systems like the primary vestibule of the auditory system (Teich, 1989), the presence of the fractal behavior throughout various brain regions suggests that the fractal behavior found in SCN neurons is a general feature of neurons, rather than a specific one pertaining to the SCN. Yet, the fractal property in SCN neurons might be potentially important, because SCN neurons exhibit the cell-autonomous circadian rhythm in the mean firing rate. Thus, the fractal behavior (or long-term correlations among ISIs) might be needed to make individual SCN neurons fire in a circadian fashion (The stochastic renewal processes alone are definitely not capable of producing the circadian modulation).

The SCN studies using theoretical models have been intensively focusing on elucidating the synchronization and entrainment properties of the SCN. Rhythmic modulation of the SCN has been described using the simple limit cycle model (Pavlidis, 1967; Goldbeter, 1995; Leloup et al., 1999; Goldbeter, 2003; Forger et al., 2003) or the modified van der Pol oscillator model (Wever, 1972; Kronauer, 1990; Jewett and Kronauer, 1998). Furthermore, observations that individual SCN neurons oscillate with dispersed periods (Liu et al., 1997) led to the development of a model of coupled self-sustained oscillators in which the SCN consists of weakly coupled, independent oscillators (Achermann and Kunz, 1999; Antle et al., 2003). All these models are based on intracellular transcription-translation feedback loops in a circadian fashion in which the protein products of the clock genes regulate their own transcription in Drosophila and Neurospora or in mammals. However, firing activity of SCN neurons on a short time scale is quite different from that of a simple periodic oscillator. How the complex spontaneous spiking activity of individual SCN neurons eventually leads to the long-range circadian rhythm and the synchronization is unknown. However, recent finding that treatment with TTX distorted cell synchrony and suppressed clock gene expression of the SCN (Yamaguchi et al., 2003) suggests that action potentials might be crucial both for intercellular synchronization and for maintaining the cell-autonomous circadian oscillation in the SCN. Thus, the dynamics and behavior of complex spiking patterns of SCN neurons should be further investigated to obtain a deeper understanding of the synchronization among SCN neurons as well as the spike generation mechanism of individual SCN neurons.

Appendix

1. Stochastic Point Process

The statistical behavior of a neural spike train can be studied by replacing the complex waveform of an individual action potential by the time interval between the peaks of successive action potentials. In mathematical terms, it is then viewed as a point process. Some point processes exhibit no dependencies among their interspike intervals (ISIs), in which case the ISI sequence obeys independent and identical distributions. Such a process is called a renewal process. Since the renewal process lacks temporal correlations, its statistical properties are completely characterized only by the shape of ISI histogram (Cox and Lewis, 1966; Tuckwell, 1989).

The homogeneous Poisson process (HPP) is the simplest renewal point process in which occurrence of an

event at any time is independent of the presence of events at other time. Because of this property, the intervals form sequences of independent, identically distributed random variables. The ISI probability density function for the HPP assumes the exponential form

$$p_\tau(\tau) = \lambda \exp(-\lambda\tau), \tag{2}$$

where λ is the mean number of events per unit time. The mean and standard deviation of ISI are readily calculated to be $<\tau> = 1/\lambda$ and $\sigma_\tau = 1/\lambda$, respectively, and the coefficient of variation (CV), defined as the standard deviation divided by the mean, is therefore $\sigma_\tau/<\tau> = 1$. The HPP serves as a benchmark against which other point processes are measured and thus plays the role that the white Gaussian process plays in the realm of continuous-time stochastic processes (Teich et al., 1997).

The dead-time-modified Poisson point process (DTMP) is a modified version of the HPP having a dead-time (refractory) interval imposed after the occurrence of each event, during which other events are prohibited from occurring. The gamma-r renewal process (GRP) is generated from the HPP by keeping only every rth event while deleting all other events. Both the DTMP and the GRP require two parameters for their description. For example, ISI probability density function of the GRP is the gamma distribution:

$$P_\tau(\tau) = \frac{(\mu r)^r \tau^{r-1} \exp(-\mu r \tau)}{\Gamma(r)}, \tag{3}$$

where μ is the mean firing rate, r is the order of the process, and the $\Gamma(r) = \int_0^\infty x^{r-1} \exp(-x)\, dx$ is the gamma function evaluated at r. The mean ISI and the standard deviation are $<\tau> = 1/\mu$ and $\sigma_\tau = 1/\mu\sqrt{r}$, respectively. Thus, the CV is $CV = 1/\sqrt{r}$. It can be either less than or greater than unity depending on the value of r. For $r < 1$, the gamma distribution is overdispersed with respect to the exponential, for which $CV = 1$. The GRP reduced to the HPP for the special case $r = 1$.

Fractal stochastic process is one example of non-renewal processes having dependencies among ISIs. This process exhibits power-law behavior of one or more statistics. The dependencies (or correlation) among ISIs generated by the fractal stochastic process can be quantified by various fractal measures.

2. Fractal Measures

2.1. Periodogram

The periodogram (PG) reveals how the power is distributed across the frequency domain. It is computed by dividing a total data set into contiguous segments of equal length T that is further divided into M equal bins. The number of events within each bin is counted and transformed into a power spectral density in the frequency range from $1/T$ to M/2T Hz. Fractal signals exhibit power-law behavior of the PG particularly in the low frequency range, whereas renewal processes present the flat PG over entire frequency regions.

2.2. Fano Factor

The Fano factor (FF) is defined as the ratio of the variance of the number of spiking events in a counting number (T) to the mean:

$$F(T) = \frac{\text{var}[N_i(T)]}{<N_i(T)>} \tag{4}$$

where $N_i(T)$ is the number of spikes in the ith counting time T. A curve is constructed by plotting the FF as a function of the counting time on a log-log plot. It reflects the degree of event clustering or anti-clustering in a point process relative to homogeneous Poisson process for which $F(T) = 1$ for all T. The FF should approach unity at sufficient small values of the T for any point process. Generally, the FF less than unity indicates that a point process is more orderly than the HPP at the particular time scale T. The FF greater than unity means increased clustering at the given time scale.

2.3. Allan Factor

The Allan factor (AF) is defined as the ratio of the event-number Allan variance to twice the mean (Allan, 1996):

$$A(T) = \frac{<[N_{i+1}(T) - N_i(T)]^2>}{2<N_i(T)>} \tag{5}$$

The FF and AF are simply related in the following equality: $A(T) = 2F(T) - F(2T)$. Like the FF, the AF is also a useful measure for the degree of event clustering in a point process compared with the HPP,

for which $A(T) = 1$ for all T. The increase in AF reflects an ordering of spike events in ever growing clusters, indicating that the ISIs are correlated over all the time scales so that each ISI depends on the entire previous activity. In the presence of scale-free fluctuations, the AF asymptotically increases as $A(T) \propto T^{\alpha_A}$. The exponent α_A is bounded to the range $0 < \alpha_A < 3$.

3. Fractal-Binomial-Noise-Driven Doubly Stochastic Gamma Point Process (FBNDG) Model

Our model, the FBNDG, generates an ISI sequence from the GRP whose firing rate is modulated by fractal stochastic noise to impose long-term correlation among ISIs. This type of model was first proposed by Teich et al. (1997) to describe the neural spike train of the visual nervous system of the cat. Two parameters, μ and r, for the GRP are estimated using the mean firing rate and CV of the experimental data ($r_{\text{model}} = 1/CV^2_{\text{exp}}$ and $\mu_{\text{model}} = \mu_{\text{exp}}$).

The long-term fractal fluctuation of the firing rate in the model is generated using the sum of K alternating binary fractal processes that is allowed to have a value of 0 or h (Fig. 7). To generate each constituent fractal point process, an ISI probability density function obeying a power-law behavior is formulated:

$$P(T) = cT^{-(1+\alpha)} \quad \text{for } A < T < B \tag{6}$$

where α is the fractal exponent, c is a normalization factor, and A and B denote lower and upper cutoff times of the correlation. Appropriate values drawn from experimental results are assigned to the five parameters (α, A, B, K, h). Since the fluctuated firing rate is made by stacking K number of the fractal process that alternatively switch between two different states (height) of 0 or h with equal probability, we set the following equality:

$$Kh/2 = \mu. \tag{7}$$

The A and B are decided as 10–50 and 10^5 (24 hrs), respectively. The number of the fractal process stacked, K, is 40 in this study. The exponent of the scale-free probability function a is set equal to the aF of the SCN neurons. The schematic diagram of the algorithm generating the ISI sequences of the FBNDG is presented in Fig. 7.

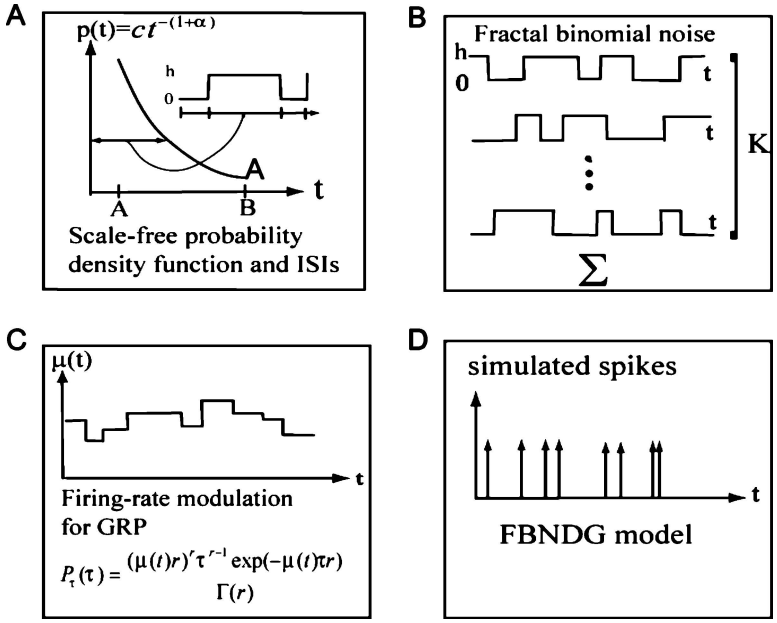

Figure 7. A schematic diagram for constructing the FBNDG model. A: the scale-free probability density function provides time series of ISIs to generate two-states (0 and h) alternating sequence. B: K numbers of those alternating sequences are summed up. C: The summation leads to the modulated firing rate, which is substituted into the GRP model. D: Then FBNDG model is constructed to produce a simulated ISI sequence.

Acknowledgment

This study was supported by Creative Research Initiatives of the Korean Ministry of Science and Technology.

References

Achermann P, Kunz H (1999) Modeling circadian rhythm generation in the suprachiasmatic nucleus with locally coupled self-sustained oscillators: Phase shifts and phase response curves. Journal of Biological Rhythms 14: 460–468.

Allan DW (1966) Statistics of atomic frequency standards. Proceedings of the IEEE 54: 221–230.

Antle MC, Foley DK, Foley NC, Silver R (2003) Gates and oscillators: A network model of the brain clock. Journal of Biological Rhythms 18: 339–350.

Colwell CS (2000) Rhythmic coupling among cells in the suprachiasmatic nucleus. Journal of Neurobiology 43: 379–388.

Cox DR, Lewis PAW (1966) The Statistical Analysis of Series of Events. Wiley, New York, pp. 17–36.

Forger DB, Dean DA 2nd, Gurdziel K, Leloup JC, Lee C, Von Gall C, Etchegaray JP, Kronauer RE, Goldbeter A, Peskin CS, Jewett ME, Weaver DR (2003) Development and validation of computational models for mammalian circadian oscillators. OMICS A Journal of Integrative Biology 7: 387–400.

Gillette MU (1991) SCN electrophysiology in vitro: Rhythmic activity and endogenous clock properties. In: DC Klein, RY Moore, SM Reppert, eds. Suprachiasmatic Nucleus: The Mind's Clock, Oxford University Press, New York, NY, pp. 125–143.

Goldbeter A (1995) A model for circadian oscillations in the Drosophila period protein (PER). Proceeding of Rotal Society in Lond B Biological Science 261: 319–324.

Gruneis F, Nakao M, Mizutani Y, Yamamoto M, Meesmann M, Musha T (1993) Further study on 1/f fluctuations observed in central single neurons during REM sleep. Biological Cybernetics 68: 193–198.

Inouye ST, Kawamura H (1979) Persistence of circadian rhythmicity in a mammalian hypothalamic "island" containing the suprachiasmatic nucleus. Proceedings of National Academy of Sciences USA 76: 5962–5966.

Jagota A, de la Iglesia HO, Schwartz WJ (2000) Morning and evening circadian oscillations in the suprachiasmatic nucleus in vitro. Nature Neuroscience 3: 372–376.

Jeong J, Kwak Y, Kim YI, Lee KJ (submitted) Temporal dynamics underlying spiking patterns of the rat suprachiasmatic nucleus in vitro.

Jewett ME, Kronauer RE (1998) Refinement of a limit cycle oscillator model of the effects of light on the human circadian pacemaker. Journal of Theoretical Biology 192: 455–465. Erratum in: J Theor Biol 1998, 194: 605.

Kelly OE, Johnson DH, Delgutte B, Cariani P (1996) Fractal noise strength in auditory-nerve fiber recordings. Journal of the Acoustical Society of America 99: 2210–2220.

Kronauer RE (1990) A quantitative model for the effects of light on the amplitude and phase of the deep circadian pacemaker, based on human data. In JA Horne, ed. Sleep'90. Ponrenagel, Bocunm, Germany, pp. 306–309.

Kumar AR, Johnson DH (1993) Analyzing and modeling fractal intensity point processes. Journal of the Acoustical Society of America 93: 3365–3373.

Läuger P (1988) Internal motions in proteins and gating kinetics of ionic channels. Biophysical Journal 53: 877–884.

Leloup JC, Goldbeter A (2003) Toward a detailed computational model for the mammalian circadian clock. Proceedings of National Academy of Science in USA 100: 7051–7056.

Leloup JC, Gonze D, Goldbeter A (1999) Limit cycle models for circadian rhythms based on transcriptional regulation in Drosophila and Neurospora. Journal of Biological Rhythms 14: 433–448.

Levine MW (1980) Firing rate of a retinal neuron is not predictable from interspike interval statistics. Biophysical Journal 30: 9–25.

Lewis CD, Gerard LG, Peter DL, Susan MB (2001) Long-term correlations in the spike trains of medullary sympathetic neurons. Journal of Neurophysiology 85: 1614–1622.

Liebovitch LS, Koniarek JP (1992) Ion channel kinetics. Protein switching between conformational states is fractal in time. IEEE Engineering in Medicine and Biology 11: 53–56.

Liebovitch LS, Toth TI (1991) A model of ion channel kinetics using deterministic chaotic rather than stochastic processes. Journal of Theoretical Biology 148: 243–267.

Liebovitch LS, Toth TI (1990) Using fractals to understand the opening and closing of ion channels. Annals of Biomedical Engineering 18: 177–194.

Linkenkaer-Hansen K, Nikouline VV, Palva JM, Ilmoniemi RJ (2001) Long-range temporal correlations and scaling behavior in human brain oscillations. Journal of Neuroscience 21: 1370–1377.

Linkenkaer-Hansen K, Nikulin VV, Palva JM, Kaila K, Ilmoniemi RJ (2004) Stimulus-induced change in long-range temporal correlations and scaling behaviour of sensorimotor oscillations. European Journal of Neuroscience 19: 203–211.

Liu C, Weaver DR, Strogatz SH, Reppert SM (1997) Cellular construction of a circadian clock: Period determination in the suprachiasmatic nuclei. Cell 91:855–860.

Longtin A (1993) Nonlinear forecasting of spike trains from sensory neurons. International Journal of Bifurcation and Chaos 3: 651–661.

Lowen SB, Teich MC (1993) Fractal renewal processes. IEEE Transactions in Information Theory 39: 1669–1671.

Lowen SB, Liebovitch LS, White JA (1999) Fractal ion-channel behavior generates fractal firing patterns in neuronal models. Physical Review E 59: 5970–80.

Lowen SB, Teich MC (1996) The periodogram and Allan variance reveal fractal exponents greater than unity in auditory-nerve spike trains. Journal of the Acoustical Society of America 99: 3585–3591.

Lowen SB, Cash SS, Poo M, Teich MC (1997) Quantal neurotransmitter secretion rate exhibits fractal behavior. Journal of Neuroscience 17: 5666–5677.

Lowen SB, Ozaki T, Kaplan E, Saleh BEA, Teich MC (2001) Fractal features of dark, maintained, and driven neural discharges in the cat visual system. Methods 24: 377–394.

Marom S (1998) Slow changes in the availability of voltage-gated ion channels: Effects on the dynamics of excitable membranes. Journal of Membrane Biology 161: 105–113.

Meijer JH, Rietveld WJ (1989) Neurophysiology of the suprachiasmatic circadian pacemaker in rodents. Physiological Reviews 69: 671–707.

Millhauser GL, Salpeter EE, Oswald RE (1988) Diffusion models of ion-channel gating and the origin of power-law distributions from single-channel recording. Proceedings of National Academy of Science 85: 1503–1507.

Moore RY, Speh JC (1993) GABA is the principal neurotransmitter of the circadian system. Neuroscience Letters 150: 112–116.

Morin LP (1994) The circadian visual system. Brain Research Reviews 19: 102–127.

Newman GC, Hospod FE, Patlak CS, Moore RY (1992) Analysis of in vitro glucose utilization in a circadian pacemaker model. Journal of Neuroscience 12: 2015–2021.

Okamura H, Berod A, Julien JF, Geffard M, Kitahama K, Mallet J, Bobillier P (1989) Demonstration of GABAergic cell bodies in the suprachiasmatic nucleus: in situ hybridization of glutamic acid decarboxylase (GAD) mRNA and immunocytochemistry of GAD and GABA. Neuroscience Letter 102: 131–136.

Pavlidis T (1967) A model for circadian clocks. Bulletin in Mathematical Biophysics 29: 781–791.

Pennartz CM, Bierlaagh MA, Geurtsen AM (1997) Cellular mechanisms underlying spontaneous firing in rat suprachiasmatic nucleus: Involvement of a slowly inactivating component of sodium current. Journal of Neurophysiology 78: 1811–1825.

Pennartz CM, De Jeu MT, Geurtsen AM, Sluiter AA, Hermes ML (1998) Electrophysiological and morphological heterogeneity of neurons in slices of rat suprachiasmatic nucleus. Journal of Physiology 506: 775–793.

Powers NL, Salvi RJ (1992) In: Abstracts of the XV Midwinter Reseach Meeting, Association for Research in Otolaryngology 292, p. 101.

Reppert SM, Weaver DR (2001) Molecular analysis of mammalian circadian rhythms. Annual Review of Physiology 63: 647–676.

Reppert SM, Weaver DR (2002) Coordination of circadian timing in mammals. Nature 418: 935–941.

Schaap J, Pennartz CM, Meijer JH (2003) Electrophysiology of the circadian pacemaker in mammals. Chronobiology International 20:171–188.

Schreiber T, Schmitz A (2000) Surrogate data methods. Physica D 142: 346–382.

Schwartz WJ, Gross RA, Morton MT (1987) The suprachiasmatic nuclei contain a tetrodotoxin-resistant circadian pacemaker. Proceedings of National Academy of Sciences USA 84: 1694–1698.

Shen Y, Olbrich E, Achermann P, Meier PF (2003) Dimensional complexity and spectral properties of the human sleep EEG. Clinical Neurophysiology 114: 199–209.

Shirakawa T, Honma S, Honma K (2001) Multiple oscillators in the suprachiasmatic nucleus. Chronobiology International 18: 371–387.

Soen Y, Braun E (2000) Scale-invariant fluctuations at different levels of organization in developing heart cell networks. Physical Review E 61: R2216–R2219.

Steedman WM, Zachary S (1990) Characteristics of background and evoked discharges of multireceptive neurons in lumbar spinal cord of cat. Journal of Neurophysiology 63: 1–15.

Steedman WM, Iggo A, Molony V, Korogod S, Zachary S (1983) Statistical analysis of ongoing activity of neurones in the substantia gelatinosa and in lamina III of cat spinal cord. Quarterly Journal of Experimental Physiology 68: 733–746.

Teich MC, Heneghan C, Lowen SB, Ozaki T, Kaplan E (1997) Fractal character of the neural spike train in the visual system of the cat. Journal of Optical Society of America A 14: 529–546.

Teich MC (1989) Fractal character of the auditory neural spike train. IEEE Transactions in Biomedical Engineering 36: 150–160.

Toib A, Lyakhov V, Marom S (1998) Interaction between duration of activity and time course of recovery from slow inactivation in mammalian brain Na^+ channels. Journal of Neuroscience 18: 1893–1903.

Tuckwell HC (1989) Stochastic processes in the neurosciences. Society for Industrial and Applied mathematics, Philadelphia, PA.

Turcott RG, Barker PDR, Teich MC (1995) Long-duration correlation in the sequence of action potentials in an insect visual interneuron. Journal of Statistical Computation and Simulation 52: 253–271.

Van Den Pol AN, Dudek FE (1993) Cellular communication in the circadian clock, the suprachiasmatic nucleus. Neuroscience 56: 793–811.

Van Den Pol AN, Finkbeiner SM, Cornell-Bell AH (1992) Calcium excitability and oscillations in suprachiasmatic nucleus neurons and glia in vitro. Journal of Neuroscience 12: 2648–2664.

West BJ (1990) Fractal Physiology and Chaos in Medicine. World Scientific, Singapore, pp.67–78.

Wever R (1972) Virtual synchronization towards the limits of the range of entrainment. Journal of Theoretical Biology 36: 119–132.

Winfree AT (2002) Oscillating systems. On emerging coherence. Science 298: 2336–2337.

Wise ME (1981) In: Statistical Distributions in Scientific Work. Reidel, Boston, pp. 211–231.

Yamaguchi S, Isejima H, Matsuo T, Okura R, Yagita K, Kobayashi M, Okamura H (2003) Synchronization of cellular clocks in the suprachiasmatic nucleus. Science 302: 1408–1412.